Contribution from the Department of Chemistry and the Molecular Structure Center, Indiana University, Bloomington, Indiana 47405, and Department of Chemistry 0506, University of California at San Diego, La Jolla, California 92093-0506

Preparation and Properties of Mononuclear and Ferromagnetically Coupled Dinuclear Manganese Complexes with 2,2'-Biphenoxide

Ann R. Schake,[1a] Edward A. Schmitt,[1b] Andrew J. Conti,[1b] William E. Streib,[1c] John C. Huffman,[1c] David N. Hendrickson,*[,1b] and George Christou*[,1a,d]

Received July 20, 1990

The treatment of $Mn_3O(O_2CPh)_6(py)_2(H_2O)$ with 2,2'-biphenol ($biphenH_2$) and NEt_3 in MeCN leads to formation of $(NEt_3H)_2[Mn(biphen)_2(biphenH)]$ (**2**). Complex **2** crystallizes in monoclinic space group $P2_1/c$ with (at −146 °C) a = 22.830 (15) Å, b = 9.982 (6) Å, c = 19.268 (16) Å, β = 108.27 (3)°, Z = 4 and V = 4169.39 Å^3. The structure was solved by direct methods and refined to R (R_w) of 6.67% (6.14%) by using 1620 unique reflections with $F > 2.33\sigma(F)$. The structure of the anion consists of a five-coordinate, trigonal-bipyramidal Mn^{III} center ligated by two chelating biphen groups and a monodentate biphenH, the second phenoxide oxygen being protonated and not ligated to the Mn. A similar reaction system using 3,3',5,5'-tetrabromobiphenol leads to the product $(NEt_3H)_2[Mn(Br_4biphen)_2(O_2CPh)]$ (**3**) whose IR spectrum suggests its structure to be similar to **2** with a chelating (η^2) benzoate replacing the monodentate biphenH group. Treatment of complex **2** with 2,2'-bipyridine (bpy) in CH_2Cl_2 yields a black solution: layering with hexanes and storage at −20 °C leads to crystallization of $Mn_2(biphen)_2(biphenH)(bpy)_2$ (**4**) whereas storage at room temperature leads to crystallization of $(bpyH)[Mn(biphen)_2(bpy)]$ (**5**). Complex **4** crystallizes in monoclinic space group $P2_1/c$ with (at −155 °C) a = 13.373 (5) Å, b = 10.508 (4) Å, c = 39.005 (22) Å, β = 90.67 (2)°, Z = 4, and V = 5480.59 Å^3. The structure was solved by direct methods and refined to R (R_w) of 7.19% (6.83%) by using 2607 unique reflections with $F > 2.33\sigma(F)$. The complex is mixed-valence (Mn^{II}, Mn^{III}), and the structure consists of two Mn atoms bridged by two oxygen atoms from two biphen groups, the other oxygen atoms of which are terminally ligated to the Mn^{III} center. Six-coordination of the latter is completed by a chelating bpy. The Mn^{II} has a chelating bpy, and five-coordination is completed by a monodentate biphenH, the second oxygen of which is protonated as in **2**. The Mn^{II} and Mn^{III} coordination geometries are distorted square-pyramidal and octahedral, respectively. The structure of complex **5** is assumed to be a six-coordinate, distorted octahedral monomer. Variable-temperature solid-state magnetic susceptibility studies on complex **4** at 10.0 kG are reported; the effective magnetic moment, μ_{eff}/Mn_2, steadily increases from 7.12 μ_B at 302.4 K to a maximum of 8.31 μ_B at 8.00 K, and then decreases slightly to 8.24 μ_B at 5.00 K, consistent with an intramolecular ferromagnetic exchange interaction. Complex **4** is the first $Mn^{II}Mn^{III}$ complex to exhibit a ferromagnetic interaction. In order to characterize fully the ferromagnetic coupling in this complex, magnetic susceptibility data were collected in the low-temperature range (~2-15 K) at fields of 10.0, 24.5, 34.1, and 43.5 kG. All data, including that at high temperatures, were least-squares fit with a full-matrix (30 × 30) diagonalization approach. Isotropic Zeeman interactions and magnetic exchange interactions, as well as axial zero-field splitting for the Mn^{II} ($D_1\hat{S}_{z1}^2$) and Mn^{III} ($D_2\hat{S}_{z2}^2$) ions, were included as matrix elements. All data were handled well by parameters of J = +0.86 cm^{-1}, g = 1.83, D_1 = 1.0 cm^{-1}, and D_2 = −1.6 cm^{-1}. The ground state at zero field is the $m_s = -5/2$ component of the $S = 9/2$ state. In the ~5-23-kG region, the $m_s = -7/2$ component becomes the ground state, and finally above ~23 kG, the $m_s = -9/2$ component crosses over to become the ground state. This is confirmed by the saturation of the magnetization at 1.78 K and 43.5 kG. EPR spectra were recorded at 8-60 K for powdered solid samples and a CH_2Cl_2/toluene frozen solution. The spectra exhibit two main features at $g \approx 2$ and $g \approx 5$ and show little variation over the temperature range explored. The $g \approx 5$ feature shows resolved manganese hyperfine structure in the frozen-solution spectrum.

Introduction

In recent publications, we have reported our efforts to date toward the preparation of synthetic models of the photosynthetic water oxidation center (WOC) to assist in the elucidation of its nature and mode of action.[2] The WOC, functioning on the donor side of photosystem II (PSII), requires a total of four Mn atoms for activity, and the latter are to be found as a tetranuclear unit, two closely-spaced dinuclear units, or a trinuclear unit close to a mononuclear site.[3] The Mn atoms appear to be oxide-bridged, and Mn···Mn separations of 2.72 (3) and ~3.3 Å have been suggested by EXAFS data.[4] The peripheral ligation is by O- and N-based groups from amino acid side chains, viz. aspartate/glutamate carboxylates, tyrosine phenoxides, and histidine imidazoles; recent reports suggest N-based ligation to Mn to be minimal, at the level of 1 ± 1 N/Mn_4, indicating predominantly O-based ligation at the native site.[5]

Our work to date has concentrated on the use of carboxylate ligands, in conjunction with N-based chelates such as 2,2'-bipyridine (bpy) or picolinate (pic$^-$, pyridine-2-carboxylate).[2] Thus, for example, the trinuclear complexes $[Mn_3O(O_2CR)_6(py)_3](ClO_4)$ (R = various) react with bpy to yield $[Mn_4O_2(O_2CR)_7(bpy)_2](ClO_4)$, and with pic$^-$ to yield products containing the $[Mn_4O_2(O_2CR)_7(pic)_2]^-$ anion. Cognizant of the fact that tyrosine phenoxide ligation to the WOC Mn atoms is a possibility, efforts have been made to incorporate phenoxide-type ligation into this chemistry. Initial work showed that treatment of $Mn_3O(O_2CPh)_6(py)_2(H_2O)$ (**1**) with phenol, p-cresol, 8-hydroxyquinoline, and 2,2-biphenol leads to $Mn_6O_2(O_2CPh)_{10}(py)_2(MeCN)_2$, the phenols functioning merely as reducing agents.[6] Better success was achieved with salicylic acid ($salH_2$, 2-hydroxybenzoic acid), which converted $Mn_3O(O_2CPh)_6(py)_2(H_2O)$ to the enneanuclear complex $Mn_9O_4(O_2CPh)_8(py)_4(sal)_4(salH)_2$; the latter contains two recognizable $[Mn_4O_2]^{8+}$ units held together via the intermediacy of an $Mn^{II}(sal)_4$ bridging unit.[7]

(1) (a) Department of Chemistry, Indiana University. (b) University of California, San Diego. (c) Molecular Structure Center, Indiana University. (d) Camille and Henry Dreyfus Teacher-Scholar, 1987-1992.

(2) (a) Vincent, J. B.; Christmas, C.; Chang, H.-R.; Li, Q.; Boyd, P. D. W.; Folting, K.; Huffman, J. C.; Hendrickson, D. M.; Christou, G. *J. Am. Chem. Soc.* **1989**, *111*, 2086. (b) Li, Q.; Vincent, J. B.; Libby, E.; Chang, H. R.; Huffman, J. C.; Boyd, P. D. W.; Christou, G.; Hendrickson, D. N. H. *Angew. Chem., Int. Ed. Engl.* **1988**, *27*, 1731. (c) Christou, G. *Acc. Chem. Res.* **1989**, *22*, 328 and references therein.

(3) (a) Govindjee; Kambara, T.; Coleman, W. *Photochem. Photobiol.* **1985**, *42*, 187. (b) Dismukes, G. C. *Photochem. Photobiol.* **1986**, *43*, 99. (c) Renger, G. *Angew. Chem., Int. Ed. Engl.* **1987**, *26*, 643. (d) Brudvig, G. W. *J. Bioenerg. Biomembr.* **1987**, *19*, 91. (e) Vincent, J. B.; Christou, G. *Adv. Inorg. Chem.* **1989**, *33*, 197.

(4) (a) Guiles, R. D.; Yachandra, V. K.; McDermott, A. E.; Cole, J. L.; Dexheimer, S. L.; Britt, R. D.; Sauer, K.; Klein, M. P. *Biochemistry* **1990**, *29*, 486 and references therein. (b) George, G. N.; Prince, R. C.; Cramer, S. P. *Science* **1989**, *243*, 789. (c) Penner-Hahn, J. E.; Fronko, R. M.; Pecoraro, V. L.; Yocum, C. F.; Betts, S. D.; Bowlby, N. R. *J. Am. Chem. Soc.* **1990**, *112*, 2549.

(5) (a) Tamura, N.; Ikeuchi, M.; Inoue, Y. *Biochim. Biophys. Acta* **1989**, *973*, 281. (b) Andreasson, L.-E. *Biochim. Biophys. Acta* **1989**, *973*, 465.

(6) Schake, A. R.; Vincent, J. B.; Li, Q.; Boyd, P. D. W.; Folting, K.; Huffman, J. C.; Hendrickson, D. N.; Christou, G. *Inorg. Chem.* **1989**, *28*, 1915.

(7) Christmas, C.; Vincent, J. B.; Chang, H.-R.; Huffman, J. C.; Christou, G.; Hendrickson, D. N. *J. Am. Chem. Soc.* **1988**, *110*, 823.

0020-1669/91/1330-3192$02.50/0

This report describes extension of our work with phenolic molecules, specifically 2,2′-biphenol (biphenH_2). It was noted above that biphenH_2 acts as a reducing agent to $Mn_3O(O_2CPh)_6(py)_2(H_2O)$, leading to a hexanuclear product; however, it was discovered that prior deprotonation of biphenol with base (NEt_3) instead leads to a Mn/biphen product, and the properties and reactivity characteristics of this species are described.

Experimental Section

Syntheses. All manipulations were carried out under aerobic conditions unless otherwise noted. Reagent grade solvents were used without further purification. 2,2′-Bipyridine (Aldrich), 2,2′-biphenol (Lancaster), and other common chemicals were used as received. 3,3′,5,5′-Tetrabromobiphenol (Br_4biphenH_2) was prepared as described in the literature.[8] Infrared spectra were recorded on Nujol mulls by using a Perkin-Elmer 203 spectrophotometer. Solution electronic spectra were recorded in the indicated solvents by using a Hewlett Packard 8450A spectrophotometer. NMR spectra were obtained at 360 MHz on a Nicolet NT-360 spectrometer. Elemental analyses were performed at the Microanalytical Laboratory, University of Manchester, or at Galbraith Laboratories, Knoxville, TN. The complex $Mn_3O(O_2CPh)_6(py)_2(H_2O)$ (**1**) was available from previous work.[9]

$(NEt_3H)_2$[Mn(biphen)$_2$(biphenH)] (2). To a solution of complex **1** (0.54 g, 0.50 mmol) in MeCN (25 cm^3) was added dropwise an MeCN solution (15 cm^3) of 2,2′-biphenol (0.60 g, 3.22 mmol) and NEt_3 (1.0 cm^3, 7.22 mmol). The resulting essentially black solution was left at ambient temperature for 24 h and then stored at −20 °C for 48 h. The black crystals that formed were collected by filtration and washed with diethyl ether; yield ca. 55%. Anal. Calcd for $C_{48}H_{57}N_2O_6Mn$: C, 70.92; H, 7.07; N, 3.45; Mn, 6.8. Found: C, 71.01; H, 7.33; N, 3.61; Mn, 6.8. IR data (cm^{-1}): 2500–2900 (s), 1590 (s), 1550 (s), 1280 (s), 1160 (m), 855 (s), 757 (s), 735 (s), 615 (s). UV/vis data [λ_{max}, nm (ϵ_m, L mol^{-1} cm^{-1})]: in $CHCl_3$, 282 (24 660), 380 (3115), 490 (2260), 655 (1115); in DMSO, 430 (2950); in CH_2Cl_2, 412 (3370), 546 (2080); in DMF, 415 (3150). Magnetic moment: solid, 4.94 μ_B; solution (DMSO), 5.30 μ_B.

$(NEt_3H)_2$[Mn(Br_4biphen)$_2$(O_2CPh)] (3). To a solution of complex **1** (0.54 g, 0.50 mmol) in MeCN (15 cm^3) was added an MeCN solution (25 cm^3) containing 3,3′,5,5′-tetrabromobiphenol (1.51 g, 3.00 mmol) and NEt_3 (1 cm^3, 7.22 mmol). A dark brown, microcrystalline powder formed almost immediately. After a few minutes, this was collected by filtration and washed with MeCN; yield, ca. 60%. Anal. Calcd for $C_{43}H_{45}N_2O_6Br_8Mn$: C, 37.4; H, 3.3; N, 2.0; Br, 46.3; Mn, 4.0. Found: C, 38.1; H, 3.2; N, 1.95; Br, 46.7; Mn, 4.0. IR data (cm^{-1}): 2500–2900 (s), 1590 (s), 1550 (s), 1255–1285 (s), 1155 (m), 1050 (s), 855 (s), 770 (s), 750 (s), 720 (s), 695 (s), 605 (m), 495 (s). UV/vis data [λ_{max}, nm (ϵ_m, L mol^{-1} cm^{-1}) in CH_2Cl_2]: 245 (60 600), 314 (22 100).

Mn_2(biphen)$_2$(biphenH)(bpy)$_2$·$^1/_2CH_2Cl_2$ (4·$^1/_2CH_2Cl_2$). To a solution of complex **2** (0.25 g, 0.31 mmol) in CH_2Cl_2 (20 cm^3) was added solid bpy (0.15 g, 0.96 mmol). Layering of the resulting essentially black solution with hexanes (20 cm^3) and storage at −20 °C produced black microcrystals in up to 90% yield on prolonged storage (2 weeks). These were collected by filtration and washed with hexanes. Anal. Calcd for $C_{56.5}H_{42}N_4O_6ClMn_2$: C, 66.6; H, 4.2; N, 5.5; Mn, 10.8. Found: C, 66.7; H, 4.3; N, 5.4; Mn, 10.4. IR data (cm^{-1}): 1590 (s), 1480 (m), 1020 (s), 1000 (w), 465 (s), 440 (m), 400 (w). UV/vis data [λ_{max}, nm (ϵ_m, L mol^{-1} cm^{-1}) in CH_2Cl_2]: 240 (33 200), 283 (32 100), 306 sh (9960), 390 (2030), 455 (1930), 642 sh (830).

(bpyH)[Mn(biphen)$_2$(bpy)]·$^1/_2CH_2Cl_2$ (5·$^1/_2CH_2Cl_2$). The previous procedure was followed to the formation of the essentially black solution. This was again layered with hexanes (20 cm^3) but this time left undisturbed at ambient temperature for 3 weeks. The resulting red-brown crystals were collected by filtration and washed with hexanes; yield ca. 55%. Anal. Calcd for $C_{44.5}H_{34}N_4O_4ClMn$: C, 68.6; H, 4.4; N, 7.2; Mn, 7.1. Found: C, 69.1; H, 4.7; N, 7.05; Mn, 7.2. IR data (cm^{-1}): 2200–3000 (br, w), 1590 (s), 1555 (w), 1290 (s), 1230 (s), 1120 (m), 1095 (m), 1055 (w), 1045 (m), 1000 (s), 965 (w), 925 (w), 855 (s). UV/vis data [λ_{max}, nm (ϵ_m, L mol^{-1} cm^{-1}) in DMF]: 337 (1470), 420 (1600). Magnetic moment in $(CD_3)_2SO$: 5.09 μ_B.

X-ray Crystallography. Data were collected on a Picker four-circle diffractometer; details of the diffractometry, low-temperature facilities, and computational procedures employed by the MSC are described elsewhere.[10a] For both complexes **2** and **4**, crystals were attached to glass fibers with a little silicone grease and then transferred to a goniostat and placed in a cold stream. Complex **4** was found to lose solvent *extremely* rapidly, however; crystals were therefore well coated with silicone grease while still in the mother liquor, affixed to the glass fiber, and transferred as quickly as possible (~5 s) to the cold stream. Even under these conditions, however, over a dozen crystals had to be examined before a suitable one was discovered.

For both samples, a systematic search of a limited hemisphere of reciprocal space located a set of diffraction maxima with symmetry and systematic absences corresponding to the unique monoclinic space group $P2_1/c$. Subsequent solution and refinement of the structures confirmed this choice. Both structures were solved by a combination of direct methods (MULTAN78) and Fourier techniques and refined by full-matrix least-squares methods.

For complex **2**, there were 5479 unique reflections but an unusually large number of these were very weak, and only 1620 reflections had $I > 2.33\sigma(I)$. The non-hydrogen atoms were readily located, but only the Mn and its five ligated oxygen atoms were refined with anisotropic thermal parameters; all other non-hydrogen atoms were refined isotropically. All hydrogen atoms except H(57) were placed in fixed, calculated positions and included in the latter refinement cycles. The O(30)···O(43) distance of 2.568 (16) Å was clearly indicative of a hydrogen-bond interaction, suggesting nonligated O(43) to be protonated. Indeed, a difference Fourier in the latter refinement stages did reveal a peak assignable to this proton, H(57), appearing approximately equidistant from the two oxygen atoms, and it was included in this position in the final refinement cycle. The final difference Fourier was essentially featureless, the largest peak being 0.35 e/Å^3.

For complex **4**, the long c axis of 39.0 Å led to considerable difficulty with overlap of strong reflections. Near the end of the data collection, the crystal was lost due to technical problems; the limits of data collection were thus $11 > h > 0$; k; $\pm l$ for $6° \le 2\theta \le 45°$. Due to the original difficulty in finding a suitable crystal, it was decided to continue with the available data. To make matters worse, the small crystal size and the increased background scattering due to the large amount of silicone grease covering the crystal resulted in less than half the data being considered observed based on $F \ge 2.33\sigma(F)$. However, even with all the indicated problems, structure solution proceeded uneventfully. All non-hydrogen atoms were readily located, although only Mn and Cl atoms were refined anisotropically. Surprisingly, hydrogen atoms, including hydroxyl hydrogen atom H(47), were observed in subsequent difference Fouriers and they were included as fixed contributors in the final cycles. The final difference Fourier was essentially featureless.

Physical Measurements. Variable-temperature magnetic susceptibility data were measured by using a Series 800 VTS-50 SQUID susceptometer (SHE Corp.). The susceptometer was operated at various magnetic fields. Diamagnetic corrections were estimated from Pascal's constants and subtracted from the experimental susceptibility of the compound. The molar susceptibility vs temperature data were fit to the appropriate theoretical expression by means of a least-squares-fitting computer program.[10b] EPR spectra were recorded on powdered samples and CH_2Cl_2/toluene glasses by using a Bruker ER200 spectrometer operating at X-band frequencies (~9.44 GHz).

Results and Discussion

Syntheses. The treatment of an MeCN solution of **1** with an excess of biphenH_2/NEt_3 leads to rapid formation of a deeply colored, essentially black solution from which a black crystalline product (**2**) was obtained in good yield. It was obvious from the IR spectrum that a NEt_3H^+ salt had been obtained, and the analytical data originally led us to believe that the tris chelate $(NEt_3H)_2[Mn(biphen)_3]$ was the product. This formulation necessitates a Mn^{IV} oxidation level, which could easily be rationalized as arising from a disproportionation reaction, a common occurrence in Mn^{III} chemistry. However, a room-temperature magnetic moment determination in the solid state gave a value of 4.94 μ_B, consistent with a Mn^{III} oxidation state (the spin-only value for high-spin d^4 Mn^{III} is 4.90 μ_B), and an iodometric redox titration gave a metal oxidation state of +3. To elucidate the cause of this discrepancy, we determined the X-ray crystal structure of **2** and found the complex to be five-coordinate $(NEt_3H)_2[Mn(biphen)_2(biphenH)]$ rather than six-coordinate $(NEt_3H)_2[Mn(biphen)_3]$, one of the biphenoxide oxygen atoms being protonated and confirming a Mn^{III} oxidation state. We had not anticipated this result, given the rarity of five-coordinate Mn^{III} in a ligand system comprising primarily O- and/or N-based ligands. Structurally characterized real examples of such species (as opposed to those that are really bridged six-coordinate) include Mn(acen)X (X = various anionic ligands), Mn^{III} porphyrins with

(8) Diels, O.; Biebergeil, A. *Ber. Dtsch. Chem. Ges.* **1902**, *35*, 306.
(9) Vincent, J. B.; Chang, H.-R.; Folting, K.; Huffman, J. C.; Christou, G.; Hendrickson, D. N. *J. Am. Chem. Soc.* **1987**, *109*, 5703.
(10) (a) Chisholm, M. H.; Folting, K.; Huffman, J. C.; Kirkpatrick, C. C. *Inorg. Chem.* **1984**, *23*, 1021. (b) Schmitt, E. A. Unpublished results.

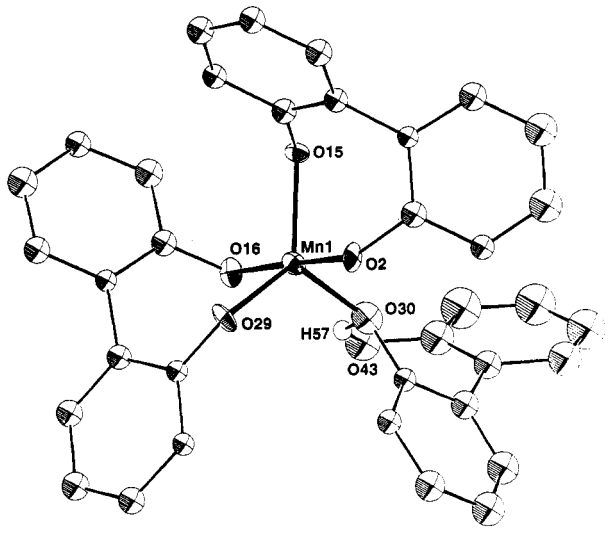

Figure 1. ORTEP representation of the anion of complex **2** at the 50% probability level. Carbon atoms are numbered sequentially from the oxygen atoms around the phenyl rings. Hydrogen atom H(57) is shown with arbitrary size.

a single axial ligand, and the Mn^{III} sites in $Mn_4O_2(OAc)_6(bpy)_2$.[11] The high-spin electronic configuration deduced from the magnetic moment is as expected for Mn^{III} in a five-coordinate environment. The electronic spectra of complex **2** in the poor donor solvents CH_2Cl_2 and $CHCl_3$ are dominated by intense absorptions assignable to LMCT, precluding analysis of the d–d bands. The spectra in DMF and DMSO are noticeably different from those in chlorinated hydrocarbons, suggesting solvent binding and an increase in coordination number to be taking place. A Mn^{III} product also results when the same procedure is employed but with tetrabromobiphenol ($Br_4biphenH_2$). In this case, however, IR and analytical data suggest the product to be $(NEt_3H)_2[Mn(Br_4biphen)_2(O_2CPh)]$ (**3**); the monoprotonated, monodentate biphenH in **2** is replaced by a $PhCO_2^-$, and the absence of an IR carboxylate band at >1600 cm^{-1} suggests the carboxylate is not monodentate but bidentate as previously confirmed crystallographically in the $[Mn(sal)_2(salH)]^{2-}$ anion.[12]

The reactivity of complex **2** to bpy has been investigated. Treatment of **2** in CH_2Cl_2 with 3 equiv of bpy yields a noticeable color change, although it is still best described as essentially black. The product obtained from this solution depends on the isolation conditions. Layering with hexanes and storage at −20 °C gives crystalline $Mn_2(biphen)_2(biphenH)(bpy)_2$ (**4**) in ~90% yield; in contrast, the same crystallization procedure at room temperature gives $(bpyH)[Mn(biphen)_2(bpy)]$ (**5**) in ~55% yield. Complex **4** is mixed-valence $Mn^{II}Mn^{III}$ whereas **5** is Mn^{III}. The formulation of **5** is supported by the IR spectrum (bipyridinium cation NH^+ stretches) and analytical data; the oxidation level is supported by the magnetic moment in DMSO (Evans method) of 5.09 μ_B. The high yield of **4** argues against a disproportionation of Mn^{III} as the source of Mn^{II}; instead, we believe the displaced biphenoxide is functioning as a reducing agent. It is not obvious why such a dramatic difference in product is observed under different crystallization temperatures; several suggestions are possible, e.g., several equilibrium species in solution, differential solubility changes with temperature, etc., but all are highly speculative. In the absence of a suitably discriminating spectroscopic handle to monitor solution species, we have not pursued this matter further. None of the complexes were found to display reversible redox processes when studied by cyclic voltammetry, nor were well-defined forward waves even observed; only very broad, ill-defined features were seen.

(11) (a) Boucher, L. J.; Day, V. W. *Inorg. Chem.* **1977**, *16*, 1360. (b) Kirner, J. F.; Scheidt, W. R. *Inorg. Chem.* **1975**, *14*, 2081. (c) Scheidt, W. R.; Lee, Y. J.; Luangdilok, W.; Haller, K. J.; Anzai, K.; Hatano, K. *Inorg. Chem.* **1983**, *22*, 1516. (d) Buchler, J. W.; Dreher, C.; Lay, K.-L.; Lee, Y. J. A.; Scheidt, W. R. *Inorg. Chem.* **1983**, *22*, 888. (e) Vincent, J. B.; Christmas, C.; Chang, H.-R.; Li, Q.; Boyd, P. D. W.; Huffman, J. C.; Hendrickson, D. N.; Christou, G. *J. Am. Chem. Soc.* **1989**, *111*, 2086.

(12) Bashkin, J. S.; Huffman, J. C.; Christou, G. Unpublished results.

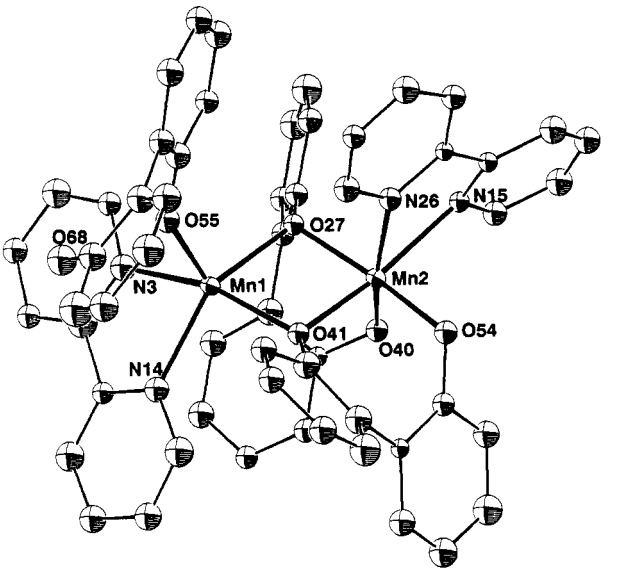

Figure 2. ORTEP representation of complex **4**. Oxygen atom O(68) is hydrogen-bonded to O(55).

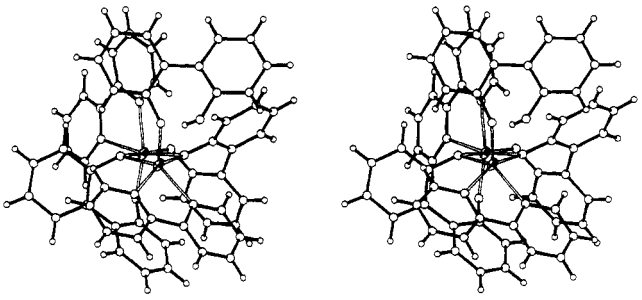

Figure 3. Stereoview of complex **4**, emphasizing the hydrogen-bonding interaction.

Table I. Crystallographic Data for Complexes **2** and **4**

	2	**4**
formula	$C_{48}H_{57}N_2O_6Mn$	$C_{59}H_{47}N_4O_6Cl_6Mn_2$
space group	$P2_1/c$	$P2_1/c$
a, Å	22.830 (15)	13.373 (5)
b, Å	9.982 (6)	10.508 (4)
c, Å	19.268 (16)	39.005 (22)
β, deg	108.27 (3)	90.65 (2)
Z	4	4
T, °C	−146	−155 °C
ρ_{calc}, g-cm^{-3}	1.295	1.489
λ, Å	0.71069	0.71069
range	$6° \le 2\theta \le 45°$	$6° \le 2\theta \le 45°$
no. of unique data	5479	6505
no. of obsd data[a]	1620	2607
R (R_w, %),[b]	6.67 (6.14)	7.19 (6.83)

[a] $F > 2.33\sigma(F)$. [b] $R = \sum||F_o| - |F_c||/\sum|F_o|$. $R_w = [\sum w(|F_o| - |F_c|)^2/\sum w|F_o|^2]^{1/2}$, where $w = 1/\sigma^2(|F_o|)$.

Description of Structures. The structure of the anion of complex **2** and the structure of complex **4** are shown in Figures 1 and 2, respectively. A stereoview of **4** is given in Figure 3. Crystallographic data are listed in Table I, and fractional coordinates and metric parameters are listed in Tables II–V.

Complex **2** crystallizes in monoclinic space group $P2_1/c$, and the asymmetric unit contains the entire anion and two NEt_3H^+ cations. The anion contains a five-coordinate Mn^{III} atom ligated by four oxygen atoms from two chelating biphen groups and one oxygen atom O(30) from the third biphen group. The second oxygen (O(43)) of the latter is protonated; the O(30)···O(43) distance is 2.57 (2) Å, indicating a hydrogen-bonded O–H···O

Table II. Selected Fractional Coordinates (×10⁴) and Thermal Parameters (Å²) for Complex **2**

atom	*x*	*y*	*z*	$10B_{iso}$
Mn(1)	7640 (1)	958 (3)	5136 (1)	14
O(2)	7333 (4)	−789 (10)	4876 (5)	18
C(3)	6920 (7)	−1096 (17)	4221 (8)	18 (3)
C(4)	6307 (7)	−1314 (15)	4158 (8)	16 (3)
C(5)	5886 (8)	−1714 (17)	3506 (9)	30 (4)
C(6)	6071 (8)	−1908 (17)	2898 (9)	29 (4)
C(7)	6681 (7)	−1685 (16)	2950 (8)	21 (3)
C(8)	7120 (6)	−1289 (14)	3604 (8)	12 (3)
C(9)	7770 (6)	−1042 (17)	3644 (7)	15 (3)
C(10)	8095 (7)	−1974 (16)	3377 (8)	20 (3)
C(11)	8697 (7)	−1795 (16)	3429 (8)	18 (3)
C(12)	8999 (7)	−649 (16)	3722 (8)	20 (4)
C(13)	8696 (7)	309 (15)	3988 (8)	16 (3)
C(14)	8070 (7)	129 (17)	3943 (8)	17 (3)
O(15)	7781 (4)	1142 (10)	4176 (5)	13
O(16)	7979 (4)	2656 (10)	5445 (5)	16
C(17)	8581 (7)	2809 (15)	5530 (8)	17 (3)
C(18)	8754 (7)	3501 (16)	4983 (8)	22 (4)
C(19)	9372 (7)	3794 (16)	5082 (8)	18 (3)
C(20)	9823 (7)	3345 (17)	5711 (9)	25 (4)
C(21)	9659 (7)	2662 (16)	6244 (8)	18 (3)
C(22)	9049 (6)	2394 (15)	6164 (8)	12 (3)
C(23)	8879 (7)	1726 (16)	6778 (8)	16 (3)
C(24)	9150 (7)	2211 (16)	7479 (8)	19 (3)
C(25)	9045 (7)	1590 (16)	8091 (8)	21 (3)
C(26)	8654 (7)	528 (15)	7978 (8)	19 (3)
C(27)	8363 (6)	44 (15)	7270 (8)	13 (3)
C(28)	8480 (6)	614 (14)	6660 (8)	12 (3)
O(29)	8227 (4)	68 (10)	5998 (5)	18
O(30)	6850 (5)	1679 (10)	5187 (5)	24
C(31)	6473 (7)	1213 (15)	5539 (8)	14 (3)
C(32)	6648 (7)	133 (16)	6030 (8)	15 (3)
C(33)	6251 (7)	−401 (16)	6383 (8)	24 (4)
C(34)	5662 (8)	145 (18)	6253 (9)	30 (4)
C(35)	5498 (7)	1196 (17)	5778 (8)	28 (4)
C(36)	5868 (7)	1749 (16)	5417 (8)	21 (4)
C(37)	5628 (7)	2868 (16)	4906 (8)	21 (3)
C(38)	4985 (8)	2900 (18)	4462 (9)	31 (4)
C(39)	4741 (8)	4007 (22)	4047 (9)	42 (4)
C(40)	5096 (9)	5096 (21)	4040 (10)	45 (5)
C(41)	5714 (9)	5126 (20)	4446 (10)	45 (5)
C(42)	5979 (8)	4022 (20)	4875 (9)	31 (4)
O(43)	6586 (5)	4157 (12)	5286 (6)	35 (3)

interaction. This is supported by a difference Fourier map that showed electron density assignable to the proton (H(57)) approximately equidistant between the two oxygens (O(30)–H(57), 1.32 Å; O(43)–H(57), 1.37 Å; O(30)–H(57)–O(43), 144.5°). The MnO_5 coordination geometry is slightly distorted trigonal bipyramidal with O(2)–Mn(1)–O(16) (176.7 (4)°) representing the axis. Equatorial–equatorial (115.5 (4)–123.9 (4)°), and axial–equatorial (84.6 (4)–94.6 (4)°) angles are close to ideal tbp values (120 and 90°, respectively). The two NEt_3H^+ cations are hydrogen-bonded to equatorial oxygen atoms O(15) and O(29) (O(15)···N(44), 2.75 (2) Å; 0(15)–H(25)–N(44), 166.7°; O(29)–N(51), 2.69 (2) Å; O(29)–H(41)–N(51), 164.8°). Since all three equatorial oxygen atoms are involved in hydrogen bonding, it is not surprising that these three Mn–O bond lengths are identical (1.973 (10)–1.984 (9) Å). The two axial Mn–O distances (1.888 (10), 1.880 (10) Å) are noticeably shorter, consistent with the nonparticipation of O(2) and O(16) in hydrogen-bonding interactions, and the nonpopulation of the d_{z^2} orbital in a d^4 tbp complex. The five Mn–O–C angles are in the range 116.4 (9)–130.0 (9)°. Since the unique biphen is ligated through only one oxygen, the unligated half of the ligand can be considered as merely a substituent in the 2-position of the ring; this viewpoint makes complex **2** the only known example of a stable, monodentate Mn^{III} phenoxide complex.

Complex **4**·$3CH_2Cl_2$ crystallizes in monoclinic space group $P2_1/c$, and the asymmetric unit contains the entire molecule and three well-separated CH_2Cl_2 solvate molecules; the latter will not be further described. The complex contains two Mn atoms bridged by two oxygen atoms (O(27) and O(41)) from two biphen groups,

Table III. Selected Fractional Coordinates (×10⁴) and Thermal Parameters for Complex **4**

atom	*x*	*y*	*z*	$10B_{iso}$
Mn(1)	5272 (2)	1403 (2)	1616 (1)	16
Mn(2)	5997 (2)	1085 (2)	847 (1)	15
N(3)	5933 (10)	898 (12)	2127 (3)	19 (3)
C(4)	6116 (12)	−304 (15)	2229 (4)	16 (3)
C(5)	6534 (13)	−606 (17)	2539 (4)	25 (4)
C(6)	6773 (12)	379 (15)	2759 (4)	19 (3)
C(7)	6577 (12)	1617 (15)	2656 (4)	16 (3)
C(8)	6134 (14)	1851 (17)	2339 (4)	26 (4)
C(9)	5974 (12)	3171 (14)	2204 (4)	13 (3)
C(10)	6229 (13)	4248 (16)	2379 (4)	24 (4)
C(11)	6097 (13)	5404 (16)	2236 (4)	22 (4)
C(12)	5671 (13)	5474 (16)	1916 (4)	22 (4)
C(13)	5389 (13)	4383 (17)	1747 (4)	25 (4)
N(14)	5538 (10)	3224 (12)	1890 (3)	18 (3)
N(15)	6626 (9)	−449 (12)	502 (3)	12 (3)
C(16)	7613 (12)	−490 (15)	414 (4)	17 (3)
C(17)	7890 (12)	−1128 (16)	122 (4)	22 (3)
C(18)	6204 (13)	−1649 (16)	2 (4)	22 (4)
C(19)	7190 (13)	−1706 (16)	−79 (4)	20 (4)
C(20)	5959 (11)	−1007 (14)	302 (4)	11 (3)
C(21)	4918 (11)	−937 (14)	424 (3)	10 (3)
C(22)	4175 (12)	−1740 (15)	319 (4)	18 (3)
C(23)	3222 (13)	−1633 (16)	470 (4)	22 (4)
C(24)	3054 (12)	−733 (14)	707 (4)	16 (3)
C(25)	3839 (13)	18 (16)	807 (4)	20 (4)
N(26)	4763 (9)	−31 (12)	673 (3)	15 (3)
O(27)	5981 (7)	120 (9)	1275 (2)	13 (2)
C(28)	6789 (12)	−634 (15)	1348 (4)	16 (3)
C(29)	6688 (13)	−1961 (15)	1287 (4)	18 (3)
C(30)	7466 (14)	7271 (17)	1387 (4)	28 (4)
C(31)	8312 (14)	−2300 (17)	1522 (4)	26 (4)
C(32)	8438 (12)	−974 (15)	1579 (4)	17 (3)
C(33)	7667 (12)	−143 (15)	1491 (4)	16 (3)
C(34)	7753 (12)	1245 (16)	1548 (4)	20 (3)
C(35)	8084 (12)	1731 (16)	1859 (4)	20 (4)
C(36)	8205 (12)	2997 (16)	1916 (4)	20 (4)
C(37)	8006 (11)	3814 (15)	1654 (4)	15 (3)
C(38)	7690 (12)	3419 (15)	1334 (4)	16 (3)
C(39)	7549 (11)	2117 (14)	1276 (4)	12 (3)
O(40)	7280 (7)	1709 (9)	953 (2)	15 (2)
O(41)	5077 (8)	2328 (9)	1139 (2)	14 (2)
C(42)	4356 (13)	3082 (16)	1019 (4)	21 (4)
C(43)	3424 (13)	3041 (15)	1150 (4)	20 (4)
C(44)	2621 (12)	3793 (16)	1026 (4)	19 (3)
C(45)	2790 (13)	4665 (16)	769 (4)	22 (4)
C(46)	3760 (14)	4772 (17)	644 (4)	29 (4)
C(47)	4541 (13)	4030 (16)	761 (4)	22 (4)
C(48)	5569 (11)	4284 (14)	642 (4)	10 (3)
C(49)	5914 (12)	5536 (16)	646 (4)	20 (4)
C(50)	6868 (13)	5842 (16)	523 (4)	24 (4)
C(51)	7428 (13)	4925 (17)	363 (4)	26 (4)
C(52)	7102 (12)	3647 (16)	356 (4)	20 (3)
C(53)	6151 (12)	3350 (15)	487 (4)	15 (3)
O(54)	5833 (8)	2123 (10)	462 (2)	16 (2)
O(55)	3939 (8)	555 (10)	1720 (2)	18 (2)
C(56)	3432 (12)	−496 (16)	1634 (4)	19 (3)
C(57)	3933 (12)	−1615 (15)	1548 (4)	16 (3)
C(58)	3408 (13)	−2700 (16)	1457 (4)	22 (4)
C(59)	2380 (13)	−2704 (16)	1459 (4)	20 (4)
C(60)	1859 (13)	−1617 (16)	1541 (4)	22 (4)
C(61)	2355 (13)	−466 (15)	1617 (4)	20 (3)
C(62)	1785 (13)	716 (16)	1654 (4)	22 (4)
C(63)	928 (13)	921 (16)	1438 (4)	25 (4)
C(64)	379 (14)	2010 (17)	1466 (5)	30 (4)
C(65)	622 (13)	2968 (17)	1700 (4)	25 (4)
C(66)	1432 (15)	2805 (19)	1918 (5)	35 (4)
C(67)	1986 (13)	1708 (16)	1901 (4)	22 (4)
O(68)	2773 (8)	1568 (11)	2132 (3)	26 (3)

the other oxygen atoms of which are terminally ligated to Mn(2) (Figure 2). Each Mn is further ligated by a terminal, chelating bpy ligand, completing six-coordination at Mn(2); five-coordination at Mn(1) is completed by a third biphen group ligating in a monodentate fashion (O(55)) as in **2**. Also, as for **2**, the second oxygen (O(68)) is protonated (H(47)), and there is a hydrogen-

Table IV. Selected Bond Distances (Å) and Angles (deg) for Complex **2**

(a) Bonds			
Mn(1)–O(2)	1.888 (10)	Mn(1)–O(29)	1.987 (9)
Mn(1)–O(15)	1.984 (9)	Mn(1)–O(30)	1.973 (10)
Mn(1)–O(16)	1.880 (10)	O(30)··O(43)	2.568 (16)
(b) Angles			
O(2)–Mn(1)–O(15)	89.6 (4)	O(15)–Mn(1)–O(29)	123.9 (4)
O(2)–Mn(1)–O(16)	176.7 (4)	O(15)–Mn(1)–O(30)	115.5 (4)
O(2)–Mn(1)–O(19)	84.6 (4)	O(16)–Mn(1)–O(29)	92.1 (4)
O(2)–Mn(1)–O(30)	94.6 (4)	O(16)–Mn(1)–O(30)	87.0 (4)
O(15)–Mn(1)–O(16)	92.3 (4)	O(29)–Mn(1)–O(30)	120.6 (4)
O(30)··H(57)··O(43)	144.5 (10)		

Table V. Selected Bond Distances (Å) and Angles (deg) for Complex **4**

(a) Bonds			
Mn(1)–O(27)	2.124 (10)	Mn(2)–O(27)	1.956 (10)
Mn(1)–O(41)	2.112 (10)	Mn(2)–O(40)	1.878 (10)
Mn(1)–O(55)	2.037 (11)	Mn(2)–O(41)	2.134 (10)
Mn(1)–N(3)	2.237 (13)	Mn(2)–O(54)	1.866 (10)
Mn(1)–N(14)	2.219 (13)	Mn(2)–N(15)	2.268 (12)
O(55)··O(68)	2.493 (18)	Mn(2)–N(26)	2.130 (13)
(b) Angles			
O(27)–Mn(1)–O(41)	78.0 (4)	O(27)–Mn(2)–N(26)	88.2 (4)
O(27)–Mn(1)–O(55)	104.2 (4)	O(40)–Mn(2)–O(41)	101.5 (4)
O(27)–Mn(1)–N(3)	103.5 (4)	O(40)–Mn(2)–O(54)	94.2 (4)
O(27)–Mn(1)–N(14)	141.1 (4)	O(40)–Mn(2)–N(15)	92.0 (5)
O(41)–Mn(1)–O(55)	106.1 (4)	O(40)–Mn(2)–N(26)	164.8 (5)
O(41)–Mn(1)–N(3)	159.7 (4)	O(41)–Mn(2)–O(54)	90.5 (4)
O(41)–Mn(1)–N(14)	92.6 (4)	O(41)–Mn(2)–N(15)	166.5 (4)
O(55)–Mn(1)–N(3)	93.3 (4)	O(41)–Mn(2)–N(26)	93.2 (4)
O(55)–Mn(1)–N(14)	114.6 (5)	O(54)–Mn(2)–N(15)	88.8 (4)
N(3)–Mn(1)–N(14)	73.5 (5)	O(54)–Mn(2)–N(26)	89.0 (5)
O(27)–Mn(2)–O(40)	90.6 (4)	N(15)–Mn(2)–N(26)	73.2 (5)
O(27)–Mn(2)–O(41)	81.3 (4)	Mn(1)–O(27)–Mn(2)	102.4 (4)
O(27)–Mn(2)–O(54)	171.2 (5)	Mn(1)–O(41)–Mn(2)	97.1 (4)
O(27)–Mn(2)–N(15)	98.4 (4)		

bonding interaction with O(55) (O(55)···O(68), 2.493 (18) Å (Figure 3); the quality of the data precludes quoting OH distances). Charge considerations necessitate a mixed-valence $Mn^{II}Mn^{III}$ description, and on the basis of structural parameters, the complex is clearly trapped-valence with Mn(2) assigned as the Mn^{III} center. There is clear evidence for a Jahn–Teller distortion at Mn(2), as expected for octahedral Mn^{III}, with N(15) and O(41) occupying axially elongated sites. Thus, Mn(2)–O(41) (2.134 (10) Å) is distinctly longer than the equatorial Mn–O distance to a bridging oxygen, Mn(2)–O(27) (1.956 (10) Å); similarly, axial Mn(2)–N(15) (2.268 (12) Å) is longer than equatorial Mn(2)–N(26) (2.130 (13) Å). In addition, bond distances to Mn(1) are distinctly longer (2.037 (11)–2.237 (13) Å) as expected for a lower oxidation state, more than compensating for the bond length *decrease* expected for the lower coordination number. The geometry at Mn(2) is distorted octahedral, while that at Mn(1) is best described as square pyramidal with O(55) at the apex, although the distortion from ideal sp geometry is somewhat severe. The $[Mn_2(\mu\text{-}O)_2]$ core is essentially planar, and asymmetric as a result of the mixed valency and its influence on the Mn–O bridging distances. The angles at the bridging oxygens are quite acute (97.1 (4), 102.4 (4)°), a point of potential relevance to the magnetic properties of **4** (vide infra). The Mn(1)···Mn(2) separation is 3.182 (6) Å.

The structure of complex **4** bears some resemblance to that of the anion in $[Mn(EtOH)_4][Mn_2(sal)_4(py)_2]$.[13] The latter contains two Mn^{III} centers bridged by two phenoxide oxygen atoms from two sal groups, the carboxylates of which are terminally ligated to the Mn. Two chelating sal and one pyridine groups complete six-coordination at each metal center. The central $Mn_2(\mu\text{-}O)_2$ planar rhomb is asymmetric, as in **4**, as a result of two Mn–O bonds being on the Jahn–Teller elongation axes. The Mn···Mn separation is 3.247 (1) Å, similar to that in **4**.

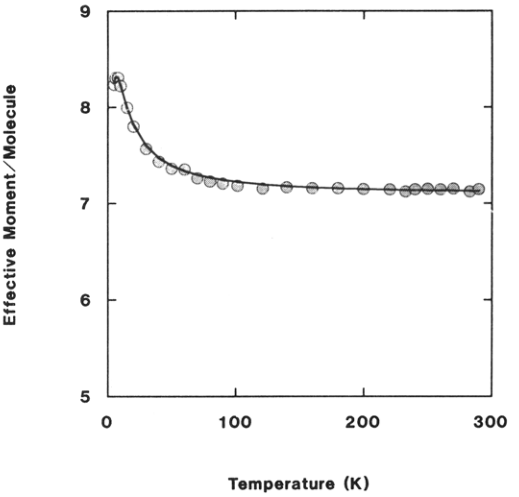

Figure 4. Plot of the effective magnetic moment, μ_{eff}/Mn_2, versus temperature for a polycrystalline sample of complex **4**·$^1/_2CH_2Cl_2$ at 10.0 kG. The solid line results from a least-squares fitting of the data to eq 1 employing a matrix diagonalization technique. See the text for fitting parameters.

Magnetochemical Data. Variable-temperature magnetic susceptibility data for complex **4**·$^1/_2CH_2Cl_2$ were obtained at 10.0 kG on a powdered crystalline sample in the temperature range 5.00–302.4 K. The effective magnetic moment per Mn_2, μ_{eff}/Mn_2, steadily increases from 7.12 μ_B at 302.4 K to a maximum of 8.31 μ_B at 8.00 K, and then decreases slightly to 8.24 μ_B at 5.00 K (Figure 4). The observed behavior is clearly indicative of an intramolecular ferromagnetic exchange interaction between high-spin Mn centers. Preliminary fitting[14] of the 5.00–302.4 K data measured at 10.8 kG to the theoretical susceptibility equation (eq 1 in ref 15) for an isotropic magnetic exchange interaction between a Mn^{II} and a Mn^{III} ion showed that the J value is positive (ferromagnetic) and small in magnitude. The five possible states for a dinuclear complex with $S_1 = {}^5/_2$ and $S_2 = 2$ have total spins of $S = {}^1/_2, {}^3/_2, {}^5/_2, {}^7/_2$, and ${}^9/_2$. Since $|J|$ is small for complex **4**, it was realized that single-ion zero-field interactions and Zeeman interactions could be of comparable magnitude to the magnetic exchange interaction. Diagonalization of the full Hamiltonian matrix is needed. Additional data obtained at lower temperatures and higher magnetic fields were also deemed necessary. Susceptibility data were measured at 10.0 kG from 2.42–15.00 K, as well as at 24.5 kG in the 2.10–15.00 K range, at 34.1 kG in the 2.03–15.00 K range, and at 43.5 kG in the 1.78–15.00 K range. All of the experimental data and the corresponding theoretically calculated data are available in the supplementary material.

The spin Hamiltonian for a dinuclear $S_1 = {}^5/_2$, $S_2 = 2$ complex assuming an isotropic Zeeman interaction is given in eq 1. The

$$\hat{H} = g\beta H_z S_z - 2J\hat{S}_1\cdot\hat{S}_2 + D_1[\hat{S}_{z1}{}^2 - {}^1/_3 S_1(S_1+1)] + D_2[\hat{S}_{z2}{}^2 - {}^1/_3 S_2(S_2+1)] \quad (1)$$

parameter D_1 gauges the axial single-ion, zero-field interaction on the Mn^{II} ion, and D_2 gauges the axial zero-field interaction on the Mn^{III} ion. Rhombic single-ion, zero-field interactions, which are expected to be small, were neglected. It is important to note that it was also assumed that the single-ion, zero-field tensors on the two metal ions are collinear. While this is not necessarily the case, the available data do not warrant adding the three extra (angular) parameters necessary to handle any misalignment. With the present reasonably sophisticated model, there are four parameters: g, J, D_1, and D_2. A least-squares fitting computer

(13) Vincent, J. B.; Huffman, J. C.; Christou, G. *Inorg. Chem.* **1986**, *25*, 996.

(14) Bashkin, J. S.; Schake, A. R.; Vincent, J. B.; Chang, H.-R.; Li, Q.; Huffman, J. C.; Christou, G.; Hendrickson, D. N. *J. Chem. Soc., Chem. Commun.* **1988**, 700.

(15) Chang, H.-R.; Larsen, S.; Pierpont, C. G.; Boyd, P. D. W.; Hendrickson, D. N. *J. Am. Chem. Soc.* **1988**, *110*, 4565.

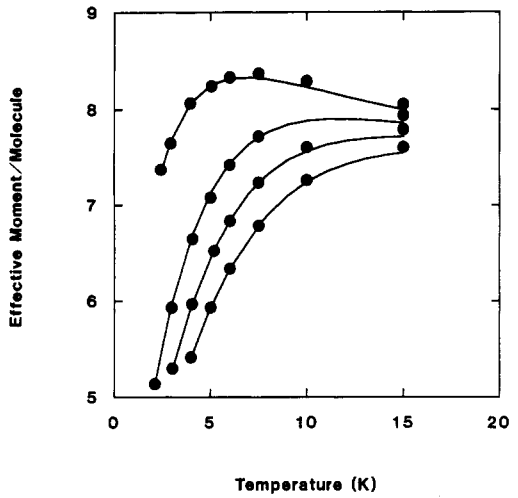

Figure 5. Plots of effective magnetic moment, μ_{eff}/Mn_2, versus temperature for complex $4 \cdot {}^1/_2CH_2Cl_2$. Four plots are shown for data collected at four different magnetic fields. The solid lines result from least-squares fitting simultaneously of data from all four fields as well as the data shown in Figure 4. A full-matrix diagonalization technique was employed. See text for parameters.

program[11] was constructed, which for each setting of these four parameters diagonalized the 30 × 30 matrix resultant from eq 1. After each diagonalization, the energies (E_i) and magnetic moments [$\delta(E_i)/\delta(H)$] of each state were used to calculate the magnetization (eq 9 in ref 2a) and consequently molar paramagnetic susceptibility as a function of temperature. An iterative least-squares routine was employed to search all of parameter space for the best fits.

The 5.00–302.4 K 10-kG data with all of the low-temperature data taken at 10.0, 24.5, 34.1, and 43.5 kG were least-squares fit together to give a very good fit; see Figures 4 and 5. The fitting parameters found are $J = +0.86$ cm^{-1}, $D_1(Mn^{II}) = +1.0$ cm^{-1}, $D_2(Mn^{III}) = -1.6$ cm^{-1}, and $g = 1.83$. The solid lines shown in Figures 4 and 5 result from this same set of parameters. It can be seen that the fit to all data is very good. Furthermore, the present J value is not very different from that (+0.89 cm^{-1}) obtained in the simpler fitting scheme.[14]

Single-ion, zero-field interaction parameters (D values) for Schiff-base and porphyrin complexes of Mn^{III} have been found[16-18] to fall in the range −1.0 to −3.0 cm^{-1}. The D_2 value from our fit is in this range. The fact that D_2 is negative indicates that the $m_s = \pm 2$ component of the $^5B_1$ ground state of a C_{4v} symmetry Mn^{III} complex is the single-ion ground state.[15] D values for Mn^{II} complexes are in the range[19-21] of 0.1 to >1.0 cm^{-1}. A positive value means that the $m_s = \pm {}^1/_2$ Kramers doublet is the ground state of a Mn^{II} complex. The signs and magnitudes of the D_1 and D_2 parameters that we obtained in our fit are reasonable. It should be noted that we did get a comparably good fit with the signs of D_1 and D_2 reversed. All of the comments about the ordering of states and magnitude of J are unchanged; however, this second fit was discounted due to the unreasonable signs of D_1 and D_2.

In Figure 6 is shown a plot of the energy versus magnetic field for the lowest lying states. The lines shown in this figure were obtained by diagonalizing the 30 × 30 Hamiltonian matrix at magnetic field intervals of 100G. The $S = {}^9/_2$ state obviously

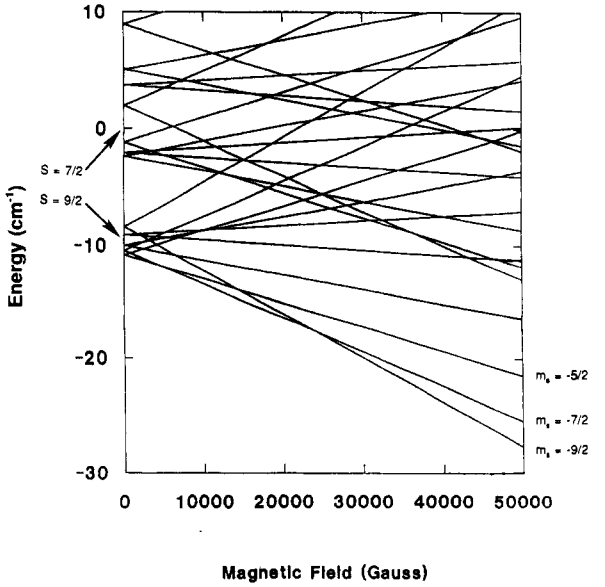

Figure 6. Plots of energy versus magnetic field for the lowest-energy states of a $Mn^{II}Mn^{III}$ complex with $J = +0.86$ cm^{-1}, $D_1(Mn^{II}) = 1.0$ cm^{-1}, and $D_2(Mn^{III}) = -1.6$ cm^{-1}.

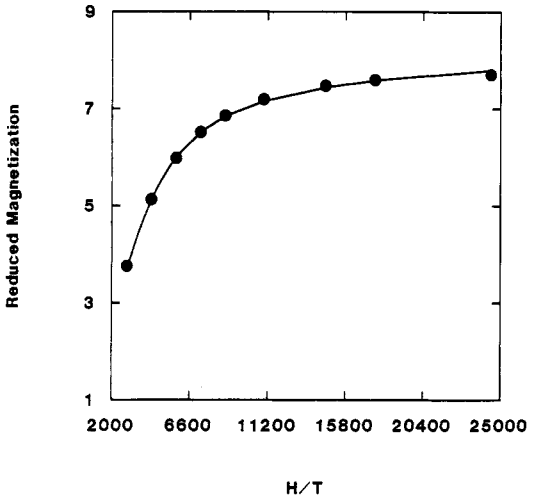

Figure 7. Plot of reduced magnetization, $M/N\beta$ (N = Avogadro's number and β = Bohr magneton) versus H/T, where H is the applied magnetic field and T is the absolute temperature.

consists of five Kramers doublets ($m_s = \pm {}^9/_2, \pm {}^7/_2, \pm {}^5/_2, \pm {}^3/_2$, and $\pm {}^1/_2$). Due to single-ion, zero-field interactions, the $\pm {}^5/_2$ component is at lowest energy when $H = 0$, followed by the $\pm {}^7/_2$, $\pm {}^3/_2$, and $\pm {}^1/_2$ components, with the $\pm {}^9/_2$ component at the highest energy for the $S = {}^9/_2$ manifold. Actually, the single-ion splitting causes considerable mixing of m_s levels. For example, the $m_s = -{}^5/_2$ levels of the $S = {}^9/_2$, ${}^7/_2$, and ${}^5/_2$ states are appreciably mixed at zero field. As can be seen in Figure 6, increasing the field from 0 to ~5 kG leads to the $m_s = {}^7/_2$ level becoming the ground state. Finally, at ~25 kG, the $m_s = -{}^9/_2$ level becomes the ground state. Thus, by the lowest temperature (1.78 K) and highest field (43.5 kG) all of the complexes populate the $m_s = -{}^9/_2$ state. This is confirmed by Figure 7, which shows a plot of reduced magnetization ($M/N\beta$, where M is magnetization, N is Avogadro's number and β is the Bohr magneton) versus the magnetic field in units of absolute temperature (i.e., H/T). The data shown in Figure 7 were obtained by keeping the field fixed at $H = 43.5$ kG while varying the temperature from 1.78 to 15.00 K. The value of $M/N\beta$ tends to "saturate" at a value of ~8 μ_B. For a $S = {}^9/_2$ state with no zero-field splitting and $g = 2$, the value of $M/N\beta$ would asymptotically approach 9 μ_B. The solid line in Figure 7 was generated with the g, D_1, and D_2 values obtained in the least-squares fit. There is no question that complex **4** has a $S = {}^9/_2$ ground state.

(16) (a) Kennedy, B. J.; Murray, K. S. *Inorg. Chem.* **1985**, *24*, 1552–1557. (b) Kennedy, B. J.; Murray, K. S. *Inorg. Chem.* **1985**, *24*, 1557–1560.
(17) Mathe, J.; Schinkel, C. J.; VanAnsted, W. A. *Chem. Phys. Lett.* **1975**, *33*, 528–531.
(18) (a) Behere, D. V.; Marathe, V. R.; Mitra, S. *Chem. Phys. Lett.* **1981**, *81*, 57–61. (b) Behere, D. V.; Mitra, S. *Inorg. Chem.* **1980**, *19*, 992–995.
(19) Yonetani, T.; Drott, H. R.; Leight, J. S., Jr.; Reed, G. H.; Waterman, M. R.; Asakura, T. *J. Biol. Chem.* **1970**, *245*, 2998.
(20) Dowsing, R. D.; Gibson, J. F.; Goodgame, M.; Hayward, P. J. *J. Chem. Soc. A* **1970**, 1133–1138.
(21) Birdy, R. B.; Goodgame, M. G. *J. Chem. Soc., Dalton Trans.* **1983**, 1469–1471.

Table VI. Structural Data for Dinuclear $Mn^{II}Mn^{III}$ Complexes

complex	Mn···Mn, Å	Mn–O–Mn, deg	J, cm^{-1}	ref
4	3.182 (6)	97.1 (4), 102.4 (4)	+0.86	*a*
$[Mn_2(bpmp)OAc)_2]^{2+}$	3.447 (1)	114.2 (2)	−6.0	22
$[Mn_2(bcmp)(OAc)_2]^{2+}$	3.422 (3)	112.1 (4)	−7.7	22
$[Mn_2(L\text{-}Im)(OAc)_2]^{2+}$	3.54 (1)	116.8 (3)	−4.5	23
Mn_2LCl_2Br	3.168 (3)	93.6 (4), 102.5 (4)	−2	15
Mn_2LBr_3	na	na	−1	15
$[Mn_2(L\text{-}py)(O_2CPh)_2]^{2+}$	3.483 (3)	116.6 (5)	−6.3	24
$[Mn_2(L\text{-}py)(OAc)_2]^{2+}$	na	na	−6.1	24

[a] This work. [b] bpmp, bcmp, L-Im, L-py and L are polydentate binucleating ligands, providing one or more endogenous bridging phenoxide oxygen atoms. na = not available.

The ferromagnetic exchange interaction and the resulting $S = {}^9/_2$ ground state observed for **4** can be contrasted with the results obtained for the few other known dinuclear $Mn^{II}Mn^{III}$ systems.[15,22-24] The exchange constants J and pertinent structural parameters (where available) are listed in Table VI for those complexes for which J values have been determined. In all cases, the magnitude of the exchange interaction is small ($|J| = 0.86$–7.7 cm^{-1}), a rationalization of which has been presented elsewhere.[22] It is noteworthy, however, that only for complex **4** is the exchange interaction found to be ferromagnetic. Since the net exchange interaction in a d^4–d^5 system will be the result of both antiferromagnetic and ferromagnetic contributions and since all interactions in Table VI are weak, we do not claim any major difference between **4** and the other complexes. The distinctly different coordination around the two Mn centers in **4**, for example, is also to be found in Mn_2LCl_2Br, albeit of a different form. Nevertheless, it is worth pointing out that the bridging phenoxide Mn–O–Mn angles do seem to correlate with the magnitude of J. The angle at the bridging oxygen would be expected to be important, for this affects the nature of σ and π overlap between the metal magnetic orbitals and the oxygen p_x, p_y, and p_z orbitals that mediate the exchange interaction. The presence of two monoatomic phenoxide bridges in **4** and Mn_2LCl_2Br (and undoubtedly also in Mn_2LBr_3) results in smaller Mn–O–Mn angles (93.6–102.5°) compared to those (112.1–116.8°) of the other complexes, which possess only one phenoxide bridge. The smaller Mn–O–Mn angles would be expected to increase the contribution to J from ferromagnetic pathways, due to the resulting near orthogonality of some of the magnetic orbitals. For Mn_2LCl_2Br and Mn_2LBr_3, therefore, the net antiferromagnetic coupling is noticeably weaker, and for complex **4**, net ferromagnetic coupling is observed.

EPR Spectroscopic Studies. The EPR activity of complex **4** was investigated in the temperature range 8–60 K for both a solid (powdered) sample and a CH_2Cl_2/toluene glass. The spectra obtained at 8 K are shown in Figure 8. The powder sample at 8 K displays two main features, an intense, broad signal at $g \approx 5$ and a weaker, broad signal at $g \approx 2$, neither of which displays any hyperfine structure. With increasing temperature, the signal intensities decrease and there is some additional broadening, but overall the 60 K spectrum is essentially unchanged compared to that at 8 K. There is, however, the appearance of a weak feature at $g \approx 12$ in the spectra at higher temperatures; this feature appears as a shoulder on the low-field side of the strong $g \approx 5$ signal. The spectrum of the CH_2Cl_2/toluene glass at 8 K looks similar to the spectrum of the powder. This suggests the molecule is retaining its solid-state structure on dissolution in this medium. There is a decrease in the line width of the $g \approx 5$ signal, allowing clear resolution of a $g \approx 12$ signal, and the appearance of a weak, broad feature at $g \approx 1.4$. Unlike the powder spectrum, some resolved hyperfine interactions (^{55}Mn, $I = {}^5/_2$) become apparent,

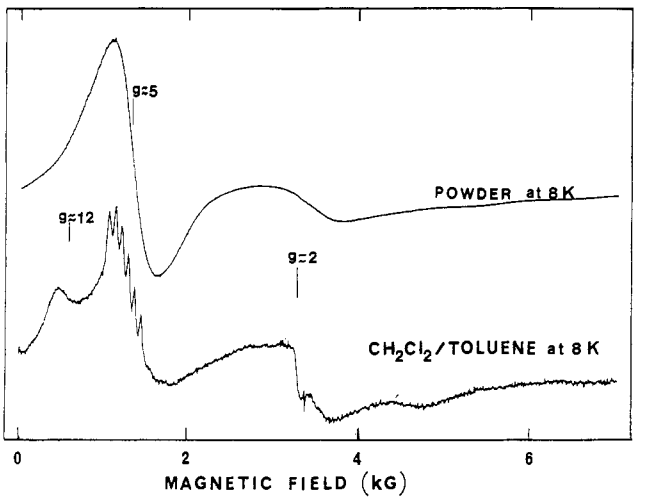

Figure 8. EPR spectra at X-band frequencies for $4 \cdot {}^1/_2CH_2Cl_2$ as a powder and in a CH_2Cl_2/toluene glass at 8 K.

but only on the $g \approx 5$ signal. A six-line pattern is clearly observable, with a peak separation of ~75 G. The features broaden and lose intensity with increasing temperature, but as observed for the powder spectrum, the overall appearance remains the same; at 60 K the $g \approx 5$ and $g \approx 2$ features are still noticeable, the former still possessing a six-line hyperfine structure. The spectra in Figure 8 are totally different from those observed for antiferromagnetically-coupled $Mn^{II}Mn^{III}$ complexes possessing $S = {}^1/_2$ ground states.[15,22-24]

Only six complexes have been reported to have a $S = {}^9/_2$ ground state. EPR spectra recorded for polycrystalline samples of two different $Cu^{II}Gd^{III}Cu^{II}$ complexes were reported[25] to exhibit several features and to be dominated by a $g = 2$ signal. These spectra were deemed too complicated to interpret. Pei et al.[26] reported X-band powder EPR data for a $Cu^{II}Mn^{II}Cu^{II}$ complex that has a $S = {}^9/_2$ ground state as a result of an antiferromagnetic exchange interaction between the Mn^{II} ion and each Cu^{II} ion. The spectrum of this complex is also dominated by an intense feature at $g = 1.99$ (3402 G). Much weaker features were observed at $g = 3.96$ (1710 G), 5.88 (1153 G), and 8.87 (764 G). The first two signals were simply assigned as the $\Delta M_S = \pm 1$ and ± 2 transitions, respectively, within the $S = {}^9/_2$ ground state.

The distorted-cubane $Mn^{IV}Mn^{III}_3$ complexes $(H_2Im)_2[Mn_4O_3Cl_6(HIm)(O_2CCH_3)_3]$[27] and $[Mn_4O_3Cl_4(O_2CCH_3)_3(py)_3]$[28] have been reported to have well-isolated $S = {}^9/_2$ ground states. The complicated EPR signals (features at low and high fields) for these two complexes have not been explained. Finally, $[L_2Fe_2(\mu\text{-}OH)_3](ClO_4)_2$ has very recently[29] been shown to have an electronically delocalized $Fe^{II}Fe^{III}$ structure with an $S = {}^9/_2$ ground state. The ligand L is *N,N',N''*-trimethyl-1,4,7-triazacyclononane. The X-band EPR spectrum for a powder sample of this complex shows a perpendicular signal at $g_\perp = 10.2$ and a weaker parallel signal at $g_\parallel = 2.3$. It was shown[29] that this is the type of EPR signal expected for an axial $S = {}^9/_2$ complex where the axial zero-field splitting of the $S = {}^9/_2$ state greatly exceeds the microwave energy. The $g_\parallel$ and $g_\perp$ signals arise from within the $\Delta M_S = \pm {}^1/_2$ Kramers doublet of the $S = {}^9/_2$ ground state.

The X-band EPR spectra shown in Figure 8 for complex **4** may be qualitatively explained by considering the effects of axial

(22) Diril, H.; Chang, H.-R.; Nilges, M. J.; Zhang, X.; Potenza, J. A.; Schugar, H. J.; Isied, S. S.; Hendrickson, D. N. *J. Am. Chem. Soc.* **1989**, *111*, 5102.
(23) Buchanan, R. M.; Oberhausen, K. J.; Richardson, J. F. *Inorg. Chem.* **1988**, *27*, 971.
(24) Suzuki, M.; Mikuriya, M.; Murata, S.; Vehara, A.; Oshio, H.; Kida, S.; Saito, K. *Bull. Chem. Soc. Jpn.* **1987**, *60*, 4305.
(25) Bencini, A.; Benelli, C.; Caneshi, A.; Dei, A.; Gatteschi, D. *Inorg. Chem.* **1986**, *25*, 572.
(26) Pei, Y.; Journaux, Y.; Kahn, O. *Inorg. Chem.* **1988**, *27*, 399.
(27) Bashkin, J. S.; Chang, H.-R.; Streib, W. E.; Huffman, J. C.; Hendrickson, D. N.; Christou, G. *J. Am. Chem. Soc.* **1987**, *109*, 6502.
(28) Li, Q.; Vincent, J. B.; Libby, E.; Chang, H.-R.; Huffman, J. C.; Boyd, P. D. W.; Christou, G.; Hendrickson, D. N. *Angew. Chem., Intl. Ed. Engl.* **1988**, *27*, 1731.
(29) Ding, X.-Q.; Bominaar, E. L.; Bill, E.; Winkler, H.; Trautwein, A. X.; Drüeke, S.; Chaudhuri, P.; Wieghardt, K. *J. Chem. Phys.* **1990**, *92*, 178.

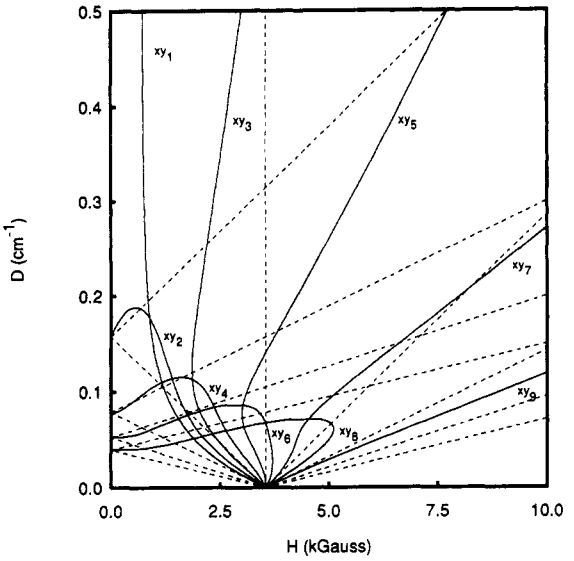

Figure 9. Resonant magnetic fields for the perpendicular (solid lines) and parallel (dashed lines) $\Delta M_S = \pm 1$ allowed EPR transitions of an $S = {}^9/_2$ spin state experiencing different values of the axial zero-field splitting parameter D.

zero-field splitting on a $S = {}^9/_2$ ground state. The 8 K powder spectrum for complex **4** looks similar to the 2.5 K powder spectrum reported for $[L_2Fe_2(\mu\text{-}OH)_3](ClO_4)_2$; however, the "$g_\perp$" signal for complex **4** appears at $g \simeq 5$, not $g \simeq 10$. This and the several additional features ($\sim$500 and $\sim$4700 G) seen in the frozen-glass spectrum of complex **4** indicate that the spectrum for this complex is more difficult to explain. As a result, we decided to generate a resonance field diagram following the general approach described by Weltner.[30] It was assumed that there is a well-isolated $S = {}^9/_2$ ground state experiencing only axial zero-field splitting ($D\hat{S}_z^2$). The magnitude of parameter D determines the number of allowed ($\Delta M_S = \pm 1$) transitions. For each value of D, two matrices were set up (each is 10×10), one for the magnetic field parallel to the molecular z axis and the other for the external field perpendicular to the z axis. The resonance fields were calculated by computing the energies of the M_S components over a grid of finely spaced values of D and H. The allowed X-band EPR transitions were found for a frequency of $\nu = 9.43$ GHz. The positions of these $\Delta M_S = \pm 1$ allowed transitions (so-called "resonance fields") are plotted in Figure 9 as a function of the parameter D. The solid lines labeled xy_1, xy_2, ..., xy_9 correspond to perpendicular transitions within and between the five Kramers doublets comprising the $S = {}^9/_2$ ground state. The dashed lines represent resonance field values for the field in the parallel orientation. Obviously, the perpendicular signals appear as much more intense spectral features. At D values that are large relative to the X-band microwave energy, only the signals occurring within the $\pm {}^1/_2$ Kramers doublet are seen with $g_\perp \simeq 10$ and $g_\parallel \simeq 2$. The solid line xy_1 corresponds to this $g_\perp$ signal at large values of D. The xy_3, xy_5, xy_7, and xy_9 lines give resonance fields within the $\pm {}^3/_2$, $\pm {}^5/_2$, $\pm {}^7/_2$, or $\pm {}^9/_2$ doublets, respectively, at large values of D. At smaller values of D, the various levels are *not* pure Kramers doublets, but are highly mixed.

The spectrum for complex **4** could possibly be interpreted in different ways by reference to Figure 9. If $D \simeq 0.1$ cm^{-1}, then the $g \simeq 12$ and $g \simeq 5$ features could be due to some overlapping of the xy_1, xy_2, xy_3, and xy_4 perpendicular transitions. At this value of D, the xy_5 resonance may be occurring in the $g \simeq 2$ feature and the broad signal at $\sim$4700 G may be due to the xy_7 resonance. Another assignment for the spectrum could be found by assuming that D was much larger than the microwave energy (i.e., above the range shown in Figure 9). In this case, the xy_1 transition would be seen. With no rhombic (E) zero-field splitting, this xy_1 signal would be seen at $g \simeq 10$. However, if $E \neq 0$, then this $g \simeq 10$ signal could split into two signals (e.g. at $g \simeq 12$ and $g \simeq 5$). With this large D value, a parallel resonance would be expected at $g \simeq 2$. In this second qualitative interpretation, the broad signal at $\sim$4700 G may be due to the xy_3 resonance field. It must be emphasized that, in order to confirm and refine the assignment of the spectrum for complex **4**, it would be mandatory to have detailed single-crystal EPR spectra for this complex. It would also be beneficial to have spectra run at higher microwave energies.

Concluding Comments

Treatment of $Mn_3O(O_2CPh)_6(py)_2(H_2O)$ (**1**) with biphenol/NEt_3 results in fragmentation of **1** and complete displacement of all ligands to yield the homoleptic complex **2**. The latter is a rare example of a five-coordinate Mn^{III} center with O- and/or N-based ligation. It is the first example of a Mn^{III} ligated to only phenoxide-like oxygen atoms and it has also proven useful as a starting point for the synthesis of other new complexes. One of these, complex **4**, is a rare example of a mixed-valence $Mn^{II}Mn^{III}$ dinuclear complex, and the first of these to exhibit ferromagnetic coupling and a resultant $S = {}^9/_2$ ground state. The complex has a large Mn···Mn separation and displays no reversible electrochemical responses; it is not, therefore, in its entirety a model for the photosynthetic water oxidation Mn_x site or, on the basis of current evidence, for *any* Mn_2 biomolecule identified to date. Nevertheless, the results described above show that it is possible to stabilize Mn^{III} in a predominantly and even completely phenoxide-based environment. It also suggests that Mn^{III}–tyrosine ligation in Mn biomolecules must continue to be entertained as a possibility in the water oxidation site and other Mn biomolecules, as indeed has already been suggested for Mn–transferrin.[31]

The results described in this report represent the initial study of the complex **1**/biphenol/NEt_3 reaction system. More recent work has unearthed an additional product containing both Mn^{III} and biphenoxide; this will be the subject of a future publication.

Acknowledgment. This work was supported by the NIH (Grants GM 39083 to G.C. and HL 13652 to D.N.H.).

Supplementary Material Available: Complete listings of crystal data, fractional coordinates, isotropic and anisotropic thermal parameters, and bond distances and angles for **2** and **4** and tables of experimental and theoretically calculated magnetic susceptibility data (28 pages); tables of observed and calculated structure factors for **2** and **4** (12 pages). Ordering information is given on any current masthead page. Complete MSC structure reports for **2** and **4** (Nos. 87148 and 87038, respectively) are available on request from the Indiana University Chemistry Library.

(30) Weltner, W., Jr. *Magnetic Atoms and Molecules*; Scientific and Academic Editions: New York, 1983.

(31) (a) Ainscough, E. W.; Brodie, A. M.; Plowman, J. E. *Inorg. Chim. Acta* **1979**, *33*, 149. (b) Scheuhammer, A. M.; Cherian, M. G. *Biochim. Biophys. Acta* **1985**, *840*, 163. (c) Keefer, R. C.; Barak, A. J.; Boycett, J. D. *Biochim. Biophys. Acta* **1970**, *221*, 390.